Available online at www.sciencedirect.com
SCIENCE DIRECT
Journal of the European Ceramic Society 26 (2006) 2307–2311
www.elsevier.com/locate/jeurceramsoc

Crystallography of Ni-doped $Zn_7Sb_2O_{12}$ and phase equilibria in the system $ZnO–Sb_2O_5–NiO$

Richard Harrington, Gabrielle C. Miles, Anthony R. West *

Department of Engineering Materials, The University of Sheffield, Mappin Street, Sheffield S1 3JD, UK

Received 13 March 2005; accepted 23 April 2005
Available online 11 July 2005

Abstract

$Zn_7Sb_2O_{12}$ forms an extensive range of Ni-containing solid solutions of formula $Zn_{7-x}Ni_xSb_2O_{12}$: $0 \leq x \leq 4$. At low x, the solid solutions are polymorphic. For $x = 0$, the low temperature β structure transforms to the high temperature α form with the spinel structure at $1225 \pm 25\,^{\circ}C$. Transition temperature decreases with increasing x and for $x \gtrsim 2$, only the α structure forms. The lattice parameter, a, of the cubic, α solid solution decreases linearly from 8.603 Å for $x = 0$ to 8.514 Å for $x = 4$. Rietveld refinement of powder neutron diffraction data for composition $x = 4$, confirmed the structural formula $Zn_3^{tet}[Ni_4Sb_2]^{oct}O_{12}$. The grain size of α depends on both composition and synthesis temperature for samples synthesised by solid state reaction at 1000–1100 °C: it increases either with decreasing x for a given reaction temperature or with increasing temperature for a given x. Sub-solidus compatibility relations in the ternary system $ZnO–Sb_2O_5–NiO$ have been determined at 1100 °C for compositions containing ≤50% Sb_2O_5.

Keywords: Varistors; X-ray methods; Transition metal oxides; Grain size; $Zn_7Sb_2O_{12}$

1. Introduction

$Zn_7Sb_2O_{12}$ is a well-known secondary phase in ZnO ceramic varistors,[1] which usually contain transition metal dopants such as Ni, Co, Mn and Cr.[2–4] Undoped $Zn_7Sb_2O_{12}$ is polymorphic with a transition at $1225 \pm 25\,^{\circ}C$[5] between the low temperature β polymorph and the high temperature α polymorph. The α polymorph has a spinel structure; structural studies on the β polymorph are currently in progress.[6] The significance of $Zn_7Sb_2O_{12}$ to varistor performance is that the α polymorph appears to act to reduce the grain size of ZnO during processing of the final ceramic; this leads to an increased number of Schottky barriers associated with grain–grain contacts and results in improved varistor action with a higher α coefficient. This coefficient α is associated with non-linearity in the current (I)–voltage (V) characteristics, given by the formula:

$$I = \left(\frac{V}{C}\right)^{\alpha} \quad (1)$$

where C is a constant.[7,8]

The significance of dopants such as Ni in $Zn_7Sb_2O_{12}$ is that they appear to act to stabilise the high temperature α polymorph in the resulting ceramics. Several studies on Ni-doped $Zn_7Sb_2O_{12}$ have been reported.[9–14] There appears to be general agreement that up to four Zn atoms can be replaced by Ni, giving the general formula $Zn_{7-x}Ni_xSb_2O_{12}$: $0 \leq x \leq 4$. In these studies, there is, however, little or no mention of the β polymorph.

Structural analyses by Rietveld refinement of X-ray powder diffraction, XRD, data have been carried out for compositions $x = 0, 1, 2, 3, 4$,[13] but the results appear not to be fully conclusive; Sb was constrained to occupy the octahedral sites and it was claimed that a small amount of Ni was present on

* Corresponding author. Tel.: +44 114 222 2000; fax: +44 114 222 5943.
E-mail address: a.r.west@sheffield.ac.uk (A.R. West).

0955-2219/$ – see front matter © 2005 Elsevier Ltd. All rights reserved.
doi:10.1016/j.jeurceramsoc.2005.04.031

the tetrahedral sites, together with Zn, for composition $x = 4$. It was also claimed that grains of two sizes were present in the samples of $x = 4$, giving a so-called bimodal distribution in grain size, but that the grains were all assumed to have the same composition. This effect was thought to be responsible for the observed broadening of the XRD peaks. From XPS data,[14] it was suggested that for $x = 4$, some of the Ni was present as Ni^{3+}, which could account for its location in tetrahedral sites.

The purpose of the present study was to clarify anomalies in the XRD data of the solid solutions, determine a phase diagram for the Ni-doped $Zn_7Sb_2O_{12}$, including variation of the α–β transition temperature with x and determine the sub-solidus compatibility relations in the ternary system $ZnO–Sb_2O_5–NiO$.

2. Experimental

The reagents were ZnO, Sb_2O_3 and $Ni(CH_3COO)_2{\cdot}4H_2O$. The ZnO (99.99% pure, Aldrich) was dried at 600 °C. The Sb_2O_3 (99.99%, Aldrich) was dried at 200 °C. The nickel acetate (98+%, Aldrich) was used undried; thermogravimetric analysis confirmed that its water content was close to 4. Starting materials were weighed out to give 1–3 g totals. These were mixed in an agate mortar and pestle with acetone, dried and fired in Pt foil boats, initially increasing the temperature slowly from room temperature to 500 °C to drive off water and decompose the nickel acetate. The samples were then removed from the furnace, reground and reheated in one of two ways. Some samples were heated directly at 1100 °C overnight. Others were heated in stages: 800 °C for 24 h, 900 °C for 24 h and then 1100 °C overnight. In general, results obtained were the same for the two heat treatments; heating to 1100 °C was necessary to achieve complete reaction. After heating at 1100 °C, some samples were heated to either higher or lower temperatures, to determine whether any changes in the phase(s) were obtained. There was no evidence of any antimony loss during heat treatment, as shown by the synthesis of phase-pure samples of $ZnSb_2O_6$ solid solutions and $Zn_7Sb_2O_{12}$ solid solutions.

It is assumed, for all samples, that oxidation of the Sb_2O_3 starting material occurs during the reactions. All the phases encountered were solid solutions based on the known phases $ZnSb_2O_6$, $NiSb_2O_6$ and $Zn_7Sb_2O_{12}$, which all contain Sb(V).

XRD was carried out with a Stoe Stadi P diffractometer, Cu $K\alpha_1$ radiation using either an image plate detector for phase analysis or a small, linear position sensitive detector for accurate lattice parameter measurements. Transmission electron microscopy (TEM) was carried out with a Philips 420 instrument, using powdered samples dispersed onto a copper grid with methanol. Powder neutron diffraction, ND, data were recorded on the HRPD instrument at the Rutherford-Appleton laboratory.

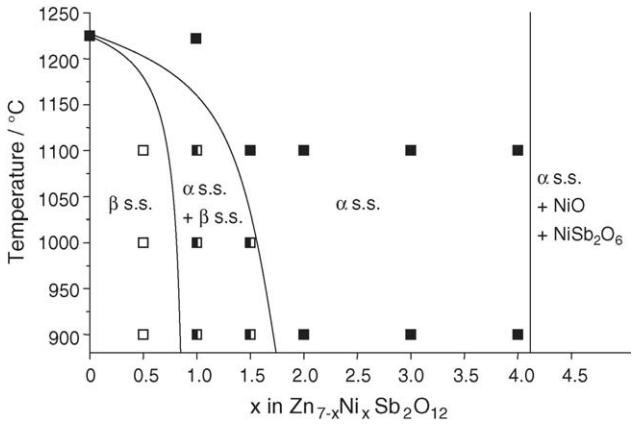

Fig. 1. Sub-solidus phase diagram for the pseudo-binary join represented by the general formula $Zn_{7-x}Ni_xSb_2O_{12}$. (□) β solid solution (ss), (◧) β ss + α ss, (■) α ss.

3. Results and discussion

3.1. $Zn_{7-x}Ni_xSb_2O_{12}$ solid solutions

Six compositions of general formula $Zn_{7-x}Ni_xSb_2O_{12}$ were prepared, as described above, with final reaction at 1100 °C for 1–2 days. Samples were removed from the furnace and allowed to cool in air. Composition $x = 0.5$ had the β structure, $x = 1.0$ was a mixture of α + β and the Ni-rich compositions with $x \geq 1.5$ had the α structure. On reheating at lower temperatures, 1000 and 900 °C, composition $x = 1.5$ developed some of the β structure giving a two phase (α + β) mixture; all other compositions were unchanged.

From these data, the pseudo-binary phase diagram shown in Fig. 1 was constructed. The β → α phase transition, which occurs at 1225 ± 25 °C in undoped $Zn_7Sb_2O_{12}$, occurs at increasingly lower temperatures with increasing Ni content. Hence, these results demonstrate that the effect of Ni is to stabilize the α phase to lower temperatures and for instance, for compositions containing $x \geq 2$, only the α polymorph is obtained. Compositions $x = 4.5$ and 5 contained a mixture of three phases, α solid solution (ss), NiO and $NiSb_2O_6$, indicating that the solid solution limit was much less than $x = 5$.

A plot of lattice parameter a against composition is shown in Fig. 2; data are very similar to those reported previously.[13] The plot is essentially linear and the data point for composition $x = 4.5$ has a very similar a value to that of $x = 4$, indicating that the solid solution limit is essentially $x = 4.0 \pm 0.2$. One literature report gives the solid solution limit as $x = 4.75$,[9] but our data clearly indicate that it is less, in agreement with other literature reports.

3.2. Structure refinement of α-$Zn_3Ni_4Sb_2O_{12}$

ND data for $x = 4$ were refined using the model of the spinel structure as a starting point. Results (Table 1; Fig. 3) confirmed: full occupancy of the octahedral sites by a random

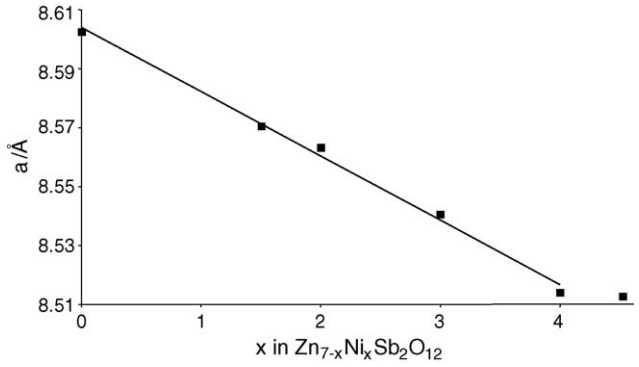

Fig. 2. Lattice parameter a vs. x for the α solid solutions, $Zn_{7-x}Ni_xSb_2O_{12}$.

Table 1
Refinement of ND data for $Zn_3Ni_4Sb_2O_{12}$

Atom	Wyckoff position	$x/y/z$	Occupancy[a]	Uiso (Å^2)
Zn	8a	0.125	0.994(5)	0.0041(4)
Ni	16d	0.5	0.668(4)	0.0024(3)
Sb	16d	0.5	0.332(4)	0.0024(3)
O	32e	0.25947(4)	1.005(2)	0.0041(3)

Bond lengths: Zn—O 1.987(2) Å, 4x; Ni/Sb—O 2.056(5) Å, 6x.

[a] Data shown are from a previous refinement cycle when all occupancies were refined simultaneously with fixed x and U. In the final refinement, occupancies were fixed as 1(Zn), 0.667(Ni), 0.333(Sb), 1(O); x for O and Uiso for all atoms were varied. Rp = 5.38, wRp = 5.09, χ^2 = 8.59 for 18 variables.

mixture of Ni and Sb, with a Ni:Sb ratio of 2:1 within one esd, as expected from the starting formula; full occupancy of the tetrahedral sites by Zn, within two esds. Hence, there is no evidence for any occupancy of the tetrahedral sites by either Sb or Ni; the latter is consistent with the octahedral site preference of Ni^{2+}; the presence of Ni as Ni^{2+} is also shown by the green colour of these solid solutions. The structural formula of this composition may therefore be written as $Zn_3^{tet}[Ni_4Sb_2]^{oct}O_{12}$.

The limiting composition of the solid solutions, $x = 4$, correlates with complete replacement of Zn on the octahedral sites by Ni. If the solid solutions were to extend beyond $x = 4$, then either Ni or Sb would have to substitute for Zn on the tetrahedral sites. This is unlikely to happen due to the strong preference for octahedral coordination of both Ni^{2+} and Sb^{5+}.

The crystallographic data reported here for $Zn_3Ni_4Sb_2O_{12}$, obtained by refinement of ND data, may be compared with those for α-$Zn_7Sb_2O_{12}$ obtained by refinement of XRD data.[5] Both contain a similar value for the oxygen x coordinate and in both the tetrahedral sites are exclusively occupied by Zn. However, the tetrahedral Zn—O bond length is smaller for $x = 4$, 1.987(2) Å, than for $x = 0$, 2.015(8) Å. The octahedral bond length is also smaller, 2.056(5) Å for $x = 4$ compared with 2.072 for $x = 0$, but this may reflect the smaller size of octahedral Ni^{2+} compared with octahedral Zn^{2+}.

3.3. Origin of XRD line broadening in α-$Zn_{7-x}Ni_xSb_2O_{12}$

According to the literature, XRD data for Ni-doped $Zn_7Sb_2O_{12}$ showed broad lines for $x = 3$ and 4 with the possibility of a bimodal distribution of grain sizes.[13] We also observed broadening of XRD lines, which depended on two parameters, composition x and heating temperature. Data are shown in Fig. 4 for samples with a range of x values all heated at 1100 °C for 18 h. These data, for the (3 1 1) reflection, show that the peak moves to lower d-spacing with increasing x, consistent with Fig. 2. In addition, the peak becomes broader with increasing x.

In Fig. 5 is shown the effect of heating temperature for one composition, $x = 4$; it is seen clearly that the peak sharpens with increasing temperature. This effect was not reversible and, for instance, after heating a sample at 1150 °C, no change in peak width was observed on subsequently reheating the same sample at 1100 °C. The peak broadening can be attributed to the influence of particle size, t, on the XRD pattern. Using the Scherrer equation:

$$t = \frac{\lambda}{\beta \cos \theta_B} \quad (2)$$

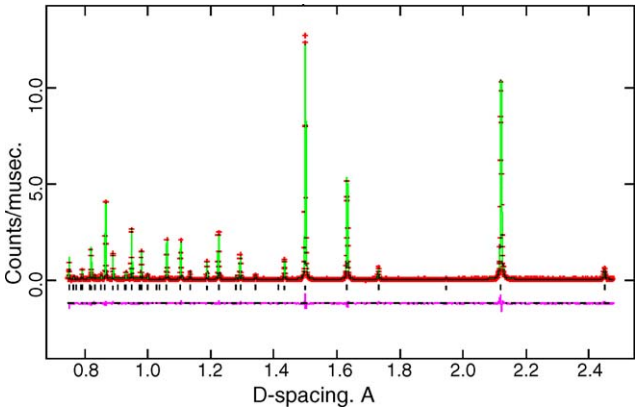

Fig. 3. Observed, calculated and difference fits from ND data collected using the back scattered detector for composition $x = 4$.

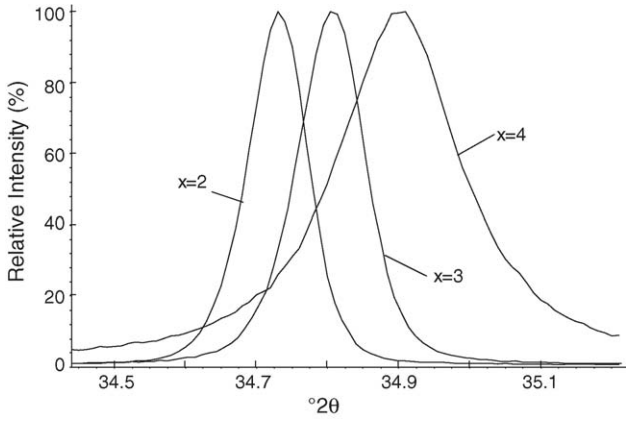

Fig. 4. XRD profile of the (3 1 1) peak for different compositions, x in the α solid solution series after heating at 1100 °C.

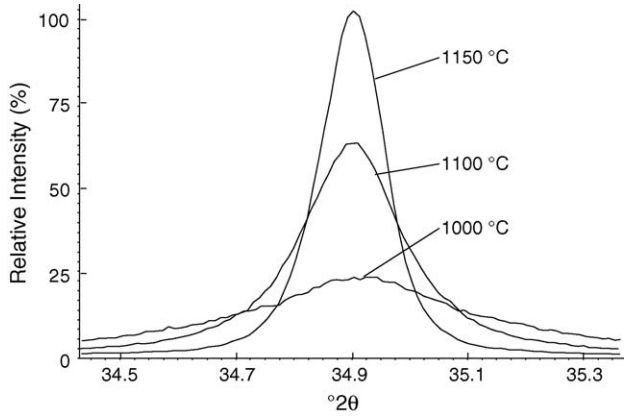

Fig. 5. XRD profile for the (3 1 1) peak for $x = 4$ after heating at different temperatures.

where λ is the X-ray wavelength, θ_B is the Bragg angle and $\beta^2 = B_M^2 - B_S^2$ where B_M, B_S are measured integral breadths (peak area divided by peak height), in radians, of the sample peak and a standard peak of a sample that is not subjected to line broadening.[15] The integral breadths of these two peaks were determined by fitting the patterns using a pseudo-Voigt function.

For each temperature, it was possible to fit the entire diffraction pattern to a single peak shape and average peak diameter with the results summarised in Table 2 for three compositions. It is clear that: (a) a single average particle size provides a very good fit to each XRD profile; (b) the particle size increases with firing temperature for a given x; and (c) the particle size increases with Zn content for a given firing temperature.

The result of TEM analysis is shown in Fig. 6 for one composition, $x = 4$ heated at 1150 °C. This shows an approximate grain size of 0.2 μm, consistent with the XRD data for which no significant line broadening was observed. TEM data (not shown) for other samples of $x = 4$ heated at lower temperatures were of poor quality, but nevertheless, showed grain sizes significantly smaller than 0.2 μm, again consistent with XRD line broadening. These results are also consistent with the observation of line broadening reported in the literature for certain samples, but the explanation is completely different: the line broadening observed here can be attributed to a particle size effect rather than to a bimodal distribution of grain sizes.

Table 2
Average grain size of α–$Zn_7Sb_2O_{12}$ solid solutions heated at different temperatures

Composition	Temperature (°C)	Average grain size (Å)
$Zn_5Ni_2Sb_2O_{12}$	1000	967 ± 100
$Zn_5Ni_2Sb_2O_{12}$	1100	≳2000
$Zn_4Ni_3Sb_2O_{12}$	1000	305 ± 20
$Zn_4Ni_3Sb_2O_{12}$	1100	≳2000
$Zn_3Ni_4Sb_2O_{12}$	1000	131 ± 20
$Zn_3Ni_4Sb_2O_{12}$	1100	375 ± 20
$Zn_3Ni_4Sb_2O_{12}$	1150	≳2000

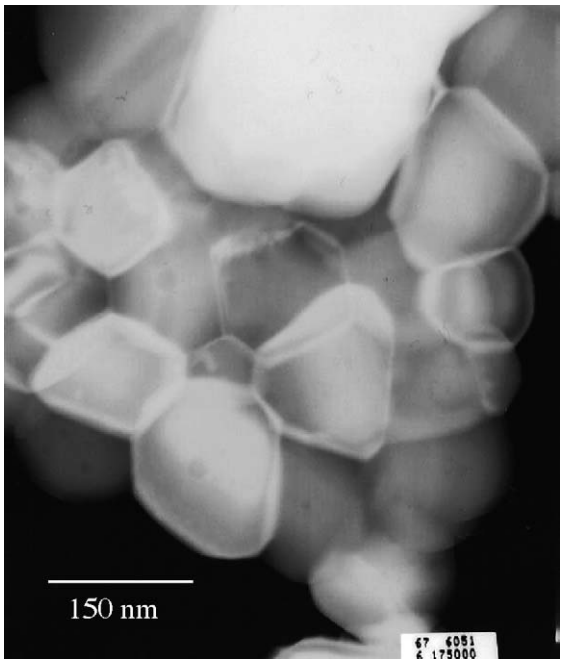

Fig. 6. TEM data for $x = 4$ heated at 1150 °C.

A possible explanation for the increased XRD line broadening in samples of high Ni content may lie in the detailed bond length changes that occur with increasing x, as follows: First the increased XRD line broadening means that it is more difficult for grain growth to occur with increasing x. Second, with increasing x, the unit cell dimension decreases, as do both tetrahedral (Zn–O) and octahedral (Zn, Ni, Sb–O) bond lengths. Third, since grain growth requires long range solid state diffusion, the shorter bonds in $x = 4$, associated with greater bond strengths for, in particular Zn^{2+} and Sb^{5+}, may make it more difficult to break the Zn–O and Sb–O bonds, and therefore for solid state diffusion to occur. Fourth, diffusion rates and grain growth may therefore be increased by either raising the temperature for a given x or by decreasing x for a given temperature, as observed.

3.4. The ternary phase diagram, $ZnO–Sb_2O_5–NiO$

The sub-solidus compatibility relations in the ternary system ZnO–Sb_2O_5–NiO were determined following heat treatment experiments on 27 compositions, with the results shown in Table 3. All samples were given a final heat treatment at 1100 °C, since heat treatments restricted to lower temperatures often did not yield complete reaction. Most samples were heated at 1100 °C for 20 h, but some of the Ni-rich compositions required longer than this to achieve equilibrium. The ternary phase diagram constructed from the data in Table 3, is shown in Fig. 7. It contains three solid solution series: a complete range of solid solutions between $ZnSb_2O_6$

Table 3
Phases present at different compositions of ZnO, NiO and Sb_2O_5

%ZnO: %NiO: %Sb_2O_5	Phase(s) present at 1100 °C[a]	Time heated at 1100 °C/h
81: 6: 13	β-ss	20
75: 13: 12	α-ss + β-ss	20
69: 19: 12	α-ss	20
63: 25: 12	α-ss	20
50: 38: 12	α-ss	20
44: 44: 12	α-ss	20
38: 50: 12	α-ss	20
25: 63: 12	α-ss + ZN ss + NiO[a]	20
0: 88: 12	$NiSb_2O_6$ + NiO	20
25: 25: 50	ZN ss	20
33: 33: 33	α-ss + ZN ss	40
57: 29: 14	α-ss + ZN ss	20
41: 47: 12	α-ss + NiO ss[a]	20
20: 35: 45	α-ss + ZN ss	40
60: 15: 25	α-ss + β-ss + ZN ss	40
20: 31: 49	α-ss + ZN ss	20
65: 30: 5	α-ss + NiO ss + ZnO	20
40: 60: 0	Ni ss + ZnO	20
44: 48: 8	α-ss + NiO ss	20
70: 20: 10	α-ss + ZnO	20
10: 80: 10	α-ss + ZN ss + NiO[a]	40
50: 10:40	β-ss + ZN ss	40
52: 43: 5	α-ss + NiO ss + ZnO	20
25: 70: 5	α-ss + NiO ss	20
90: 5: 5	α-ss + β-ss + ZnO	60
31: 56: 13	α-ss + ZN ss + NiO[a]	40

α-ss = α-$Zn_{7-x}Ni_xSb_2O_{12}$; β-ss = β-$Zn_{7-x}Ni_xSb_2O_{12}$; ZN ss = $Zn_{1-x}Ni_xSb_2O_6$; NiO ss = $Ni_{1-x}Zn_xO$.

[a] Stoichiometric NiO and NiO ss, i.e. $Ni_{1-x}Zn_xO$ can be distinguished approximately from line shifts in the XRD patterns.

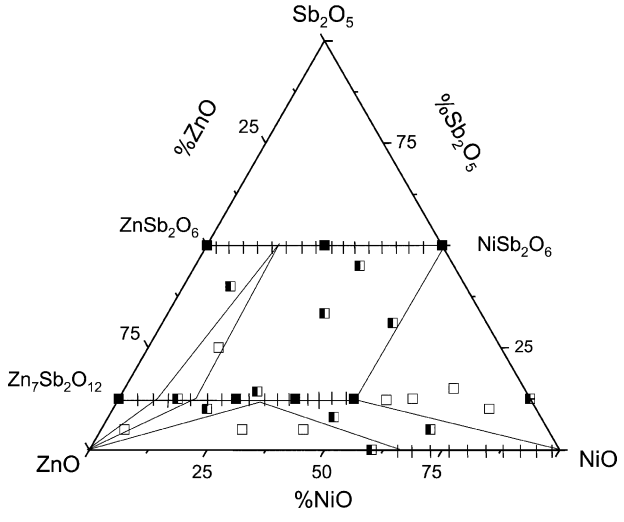

Fig. 7. Sub-solidus compatibility relations at 1100 °C; closed, half closed and open squares refer, respectively, to one-, two- and three-phase products.

and $NiSb_2O_6$; the extensive range of solid solutions based on $Zn_7Sb_2O_{12}$; NiO solid solutions containing up to 30–40% ZnO, depending on temperature.[16] The remainder of the phase diagram is divided into a number of two-phase and three-phase compatibility regions. No attempt was made to study compositions containing >50% Sb_2O_5.

4. Conclusions

- The $Zn_{7-x}Ni_xSb_2O_{12}$ solid solutions form up to a limit of $x = 4$, at which point all the Zn^{2+} on octahedral sites has been replaced by Ni^{2+}. Further substitution of Ni^{2+} into the structure would require Ni, presumably, to occupy tetrahedral sites, which is regarded as unlikely.
- Ni-rich $Zn_{7-x}Ni_xSb_2O_{12}$ solid solutions show XRD line broadening associated with small particle size for samples reacted at 1000 °C, but the line broadening decreases on increasing the reaction temperature. The increase in line broadening at high x may be associated with increased difficulty of grain growth which may be correlated with smaller unit cell dimensions and shorter metal-oxygen bond distances for solid solutions with high values of x.

Acknowledgements

We thank EPSRC for financial support, K. Knight for assistance with the HRPD measurements and H. Bagshaw for carrying out the TEM work.

References

1. Clarke, D. R., *J. Am. Ceram. Soc.*, 1999, **82**, 485–502.
2. Inada, M., *Jpn. J. Appl. Phys.*, 1979, **18**, 1439–1446.
3. Lu, C. H., Chyi, N., Wong, H. W. and Hwang, W. J., *Mater. Chem. Phys.*, 2000, **62**, 164–168.
4. Cho, S. G., Lee, H. and Kim, H. S., *J. Mater. Sci.*, 1997, **32**, 4283–4287.
5. Miles, G. C. and West, A. R., *J. Am. Ceram. Soc.*, 2005, **88**(2), 396–398.
6. Miles, G. C., Kirk, C. A. and West, A. R., In preparation.
7. Gupta, T. K., *J. Am. Ceram. Soc.*, 1990, **73**, 1817–1840.
8. Inada, M., *Jpn. J. Appl. Phys.*, 1980, **19**, 409–419.
9. Yoshida, T., Nakamura, H. and Ohtsuka, A., *Yogyo Kyokai Shi*, 1985, **93**, 117–122.
10. Poleti, D., Vasovic, D., Karanovic, L. and Brankovic, Z., *J. Solid State Chem.*, 1994, **112**, 39–44.
11. Poleti, D. and Karanovic, L., *J. Serb. Chem. Soc.*, 1998, **63**, 661–668.
12. Lisboa, P. N., Gama, L., Paiva-Santos, C. O., Varela, J. A., Ortiz, W. A. and Longo, E., *Mater. Chem. Phys.*, 2000, **65**, 208–211.
13. Gama, L., Paiva-Santos, C. O., Vila, C., Lisboa-Filho, P. N. and Longo, E., *Powder Diffraction*, 2003, **18**, 219–223.
14. Lisboa, P. N., Vila, C., Goes, M. S., Morilla-Santos, C., Gama, L., Longo, E., Schreiner, W. H. and Paiva-Santos, C. O., *Mater. Chem. Phys.*, 2004, **85**, 377–382.
15. Warren, B. E., *X-ray Diffraction*. Addison-Wesley Publishing Company, 1969, pp. 251–264.
16. Bashkirov, L. A. and Bashkirova, M. G., *Inorg. Mater.*, 1971, **7**, 1972–1974.